Polytorsional-amide/carboxylates-directed Cd(II) coordination polymers exhibiting multi-functional sensing behaviors

Jie Chi,[a#] Yajun Mu,[a#] Yan Li,[a] Pengpeng Shao,[b] Guocheng Liu,[a,b*] Bin Cai,[c*] Na Xu,[a] and Yongqiang Chen[d*]

[a] *College of Chemistry and Materials Engineering, Professional Technology Innovation Center of Liaoning Province for Conversion Materials of Solar Cell, Bohai University, Jinzhou 121013, P. R. China.*

[b] *Key Laboratory of Cluster Science Ministry of Education, Beijing Key Laboratory of Photoelectronic/Electrophotonic, Advanced Research Institute of Multidisciplinary Science, School of Chemistry and Chemical Engineering, Beijing Institute of Technology, Beijing 100081, P. R. China.*

[c] *School of Chemistry and Chemical Engineerng, Zhoukou Normal Unversity, Zhoukou 466001, P.R. China.*

[d] *College of Chemistry and Chemical Engineering, Jinzhong University, Jinzhong, Shanxi, 030619, PR China.*

[#]Jie Chi and Yajun Mu contributed equally to this work.

[*]Corresponding author: E-mail: lgch1004@sina.com (Guocheng Liu), caib@actinide.org (Bin Cai)

chenjzxy@126.com (Yongqiang Chen)

Supporting Information

Materials and Methods

According to the method reported in the literature, the ligand [N,N'-bis(4-methylenepyridin-4-yl)-1,4-naphthalene dicarboxamide (**L**)] was synthesized.[S1] All reagents and solvents were obtained from commercial sources without further purification. Powder X-ray diffraction (PXRD) data were measured on a D/teX superdiffractometer (Cu-Kα, λ = 1.5406 Å). Infrared absorption spectroscopy (KBr pellet) was recorded at 296 K on a Varian 640 FT-IR spectrometer in the range 500–4000 cm^{-1}. The fluorescence spectrum was tested on a Hitachi F-4500 fluorescence spectrometer. Scanning electron microscope image was obtained on JSM-IT200. Ultraviolet-

visible absorption spectra were performed on PerkinElmer Lambda 750. The fluorescence lifetime can be obtained by using FLS1000 transient steady-state fluorescence spectrometer.

X-ray crystallography

The X-ray single crystal diffraction data for **1**–**3** were collected at 296 K on a Bruker Smart APEX II diffractometer equipped with MoKα radiation (λ = 0.71073 Å). The structures were solved by direct method and refined by full-matrix least-squares on F^2. All non-hydrogen atoms were refined anisotropically. The crystal data details of CPs **1**–**3** are shown in Table 1. Tables S1–S3 (supporting information) are the selected bond lengths (Å) and angles (deg). CCDC numbers: 2071313(**1**), 2071314(**2**), 2071312(**3**). Crystal data can be collected by www.ccdc.cam.ac.uk/conts/retrieving.html. In the crystal analysis process, CP **1** used "Solvent mask" command, CP **3** used "EQIV" and "DFIX" operations. In **3**, there are two dicarboxylates ligands in the crystal structure, and each ligand has a symmetrical center, so the independent one is half. The unit has two such semi-ligands (Ligand A: O5, O6, C1-C4 and ligand B: O1, O2, C5-C8). Ligand A is unstable and may be disordered when it is corrected. Since the synthetic raw materials contain chlorine, ligand A and chlorine were disordered, and the occupancy was corrected. The final result showed that the occupancy of ligand A was 0.758, and that of chlorine (Cl1) was 0.242.

Synthesis of 2 and 3

Preparation of $C_{31}H_{32}CdN_4O_7$ (2). $CdCl_2·5/2H_2O$ (0.0457g, 0.2mmol), **L** (0.0394g, 0.1mmol), H_2PIM (0.0320g, 0.2mmol), H_2O (6mL), NaOH (0.1mol/L, 4mL) and DMA (2mL), the mixture was placed in a 25 mL Teflon-lined stainless steel autoclave and then reacted at 120℃ for 4 days. After cooling to room temperature, colorless crystals were obtained in 26% yield based on **L**. Anal. Calcd (%) for $C_{31}H_{32}CdN_4O_7$: C 54.35, H 4.71, N 8.18. Found: C 55.33, H 4.71, N 8.19. IR (KBr, cm^{-1}): 3267w, 3043w, 2926w, 1627s, 1537s, 1420s, 1308s, 1213w ,1147w, 1013m, 968w, 912w, 778s, 628m (Fig. S1).

Preparation of $C_{31.03}H_{30.55}CdCl_{0.24}N_4O_{5.52}$ (3). The synthetic method of **3** was similar to that of **2**, except that H_2PIM was replaced by H_2SUB (0.0348g, 0.2mmol). Colorless crystals were obtained in 30% yield based on **L**. Anal. Calcd (%) for $C_{31.03}H_{30.55}CdCl_{0.24}N_4O_{5.52}$: C 55.73, H 4.57, N 8.38. Found: C 56.45, H 4.72, N 8.24. IR (KBr, cm^{-1}): 3216w, 3038w, 2915w, 1660s, 1615m, 1570w, 1532s, 1420s, 1303m, 1258w, 1219w, 1124w, 1018w, 856w, 756w, 717w (Fig.

S1).

The process of the fluorescence experiment for CPs 1–3

Because the CPs are insoluble in water, the synthesized crystals were placed in a ball-milled tube with several ball-milled balls with a particle size of 0.5 mm after air drying, distilled water was added. The ball-milled process was performed for 30 minutes and left at room temperature for one day to obtain a fine powder. The morphology of the sensing materials were carried out by SEM(Fig. S2). In the fluorescence sensing experiment, 3 mg crystal powder was soaked in cationic solution (Ba^{2+}, Ni^{2+}, Co^{2+}, Cu^{2+}, Na^{+}, Cd^{2+}, Mn^{2+}, Fe^{3+}, Zn^{2+}, K^{+}), anionic solution (OH^{-}, HCO_3^{-}, NO_3^{-}, Br^{-}, CO_3^{2-}, I^{-}, CH_3COO^{-}, MnO_4^{-}, CrO_4^{2-}, $Cr_2O_7^{2-}$) and organochlorine pesticides (AT, 1,2,3-TCB, 1,2,4,5-TCB, 2,6-DC-4-NA). Ultrasonic treatment was carried out for 40 minutes, and the suspension obtained was tested for selectivity and anti-interference. Fluorescence titration experiment can be used as the basis of quantitative analysis of analytes. 3 mg crystal powder was added into deionized water, ultrasonic for 40 minutes to form suspension, then added the solution to be tested into the prepared solution for fluorescence titration experiment, and used the instrument to test the fluorescence intensity.

Table S1 Selected bond distances (Å) and angles (°) for **1**.

1			
Cd(1)–O(4)A	2.4034(17)	O(1)–Cd(1)–N(1)	91.95(7)
Cd(1)–O(1)B	2.3321(16)	O(1)B–Cd(1)–N(1)	90.60(7)
Cd(1)–O(1)	2.3142(16)	O(1)–Cd(1)–N(4)C	90.44(7)
Cd(1)–O(3)A	2.3507(16)	O(1)B–Cd(1)–N(4)C	96.17(8)
Cd(1)–N(1)	2.3347(18)	O(3)A–Cd(1)–O(4)A	55.01(6)
Cd(1)–N(4)C	2.354(2)	O(3)A–Cd(1)–N(4)C	90.08(7)
O(1)–Cd(1)–O(4)A	139.29(5)	N(1)–Cd(1)–O(4)A	88.42(7)
O(1)B–Cd(1)–O(4)A	147.94(5)	N(1)–Cd(1)–O(3)A	89.17(6)
O(1)–Cd(1)–O(1)B	72.77(6)	N(1)–Cd(1)–N(4)C	173.21(8)
O(1)–Cd(1)–O(3)A	165.67(6)	N(4)C–Cd(1)–O(4)A	85.62(7)
O(1)B–Cd(1)–O(3)A	92.94(6)		

Symmetry code: A: $-1 + x, + y, + z$; B: $2 - x, - y, -1 - z$; C: $-1 + x, 1 + y, 1 + z$

Table S2 Selected bond distances (Å) and angles (°) for **2**.

2			
Cd(1)–O(4)A	2.3197(19)	O(1)–Cd(1)–O(1)B	71.34(8)
Cd(1)–O(1)B	2.367(2)	O(1)B–Cd(1)–O(3)A	163.66(7)
Cd(1)–O(1)	2.281(2)	O(1)–Cd(1)–O(3)A	93.81(7)
Cd(1)–O(3)A	2.4618(19)	O(1)–Cd(1)–N(1)	95.67(8)
Cd(1)–N(1)	2.329(2)	O(1)–Cd(1)–N(4)C	94.37(8)
Cd(1)–N(4)C	2.376(2)	O(1)B–Cd(1)–N(4)C	90.51(8)
O(4)A–Cd(1)–O(1)B	140.60(7)	N(1)–Cd(1)–O(1)B	92.10(8)
O(4)A–Cd(1)–O(3)A	54.36(7)	N(1)–Cd(1)–O(3)A	96.26(8)
O(4)A–Cd(1)–N(1)	86.07(8)	N(1)–Cd(1)–N(4)C	169.94(8)
O(4)A–Cd(1)–N(4)C	85.74(8)	N(4)C–Cd(1)–O(3)A	83.68(8)
O(1)–Cd(1)–O(4)A	148.03(7)		

Symmetry code: A: 2 – *x*, – *y*, 1 – *z*; B: 2 – *x*, – *y*, 2 – *z*; C: 1 + *x*, –1 + *y*, 1 + *z*

Table S3 Selected bond distances (Å) and angles (°) for **3**.

3			
Cd(1)–O(6)A	2.272(7)	N(4)A–Cd(1)–Cl(1)	92.5(3)
Cd(1)–O(2)	2.339(5)	O(2)–Cd(1)–Cl(1)	95.6(3)
Cd(1)–O(1)	2.486(5)	O(6)–Cd(1)–O(4)B	96.2(2)
Cd(1)–N(4)A	2.340(6)	N(1)–Cd(1)–O(4)B	81.25(18)
Cd(1)–N(1)	2.335(6)	N(4)A–Cd(1)–O(4)B	77.83(17)
Cd(1)–Cl(1)	2.430(11)	O(2)–Cd(1)–O(4)B	136.20(16)
Cd(1)–O(4)B	2.437(5)	Cl(1)–Cd(1)–O(4)B	127.6(3)
O(6)–Cd(1)–N(1)	81.4(2)	O(6)–Cd(1)–O(1)	170.8(2)
O(6)–Cd(1)–N(4)A	105.7(2)	N(1)–Cd(1)–O(1)	89.39(19)
N(1)–Cd(1)–N(4)A	158.49(19)	N(4)A–Cd(1)–O(1)	82.89(18)
O(6)–Cd(1)–O(2)	126.8(2)	O(2)–Cd(1)–O(1)	54.10(16)
N(1)–Cd(1)–O(2)	95.94(19)	Cl(1)–Cd(1)–O(1)	148.4(3)
N(4)A–Cd(1)–O(2)	95.69(18)	O(4)B–Cd(1)–O(1).	82.12(16)
N(1)–Cd(1)–Cl(1)	104.2(3)		

Symmetry code: A: + *x*, 1 + *y*, *z* – 1; B: 2 – *x*, 1 – *y*, 1 – *z*

The Cd–O bond length range of CPs **1**–**3** is 2.262–2.486. After sorting out the published literature, it is found that all the Cd–O bond lengths are within the normal range.[S2-S5]

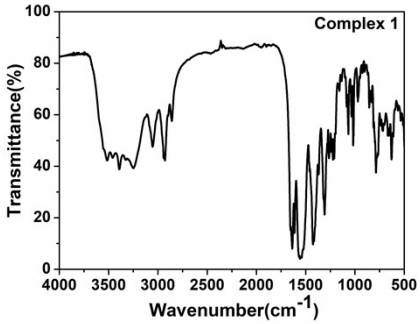

(a)

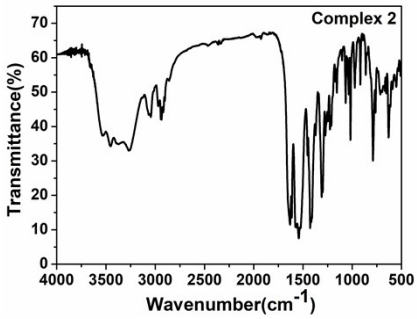

(b)

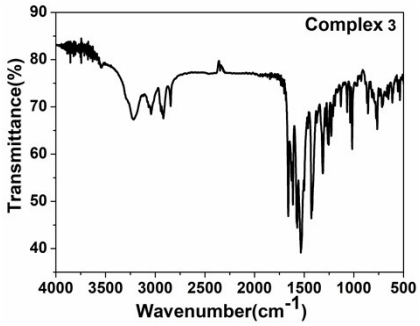

(c)

Fig. S1 The IR spectra of CPs **1**–**3**.

The infrared spectrum of CPs **1**–**3** is displayed in the frequency range of 500–4000 cm^{-1}. The characteristic peaks of –OH groups of water molecules in **1** and **2** were observed at about 3300–3500 cm^{-1}.[S6] The peaks in the range of 2800–3300 cm^{-1} were mainly attributed to $–CH_2–$ in carboxylic acid groups and ligand **L**. For the $\nu_{C=O}$ vibration of amide group, strong bands appeared at 1632 cm^{-1}, 1627 cm^{-1}, 1660 cm^{-1} in CPs **1**–**3**, respectively.[S7] The vibration range of naphthalene ring skeleton is 1400–1600 cm^{-1}.[S8]

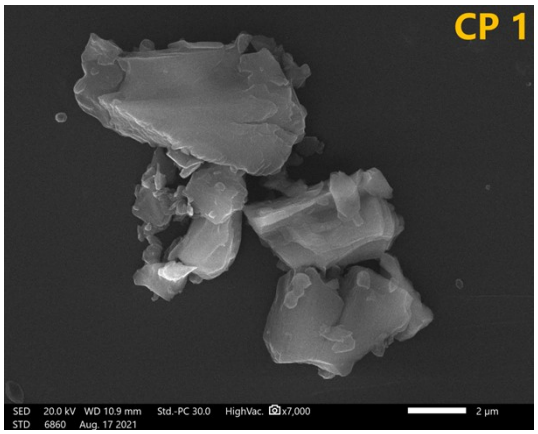

(a)

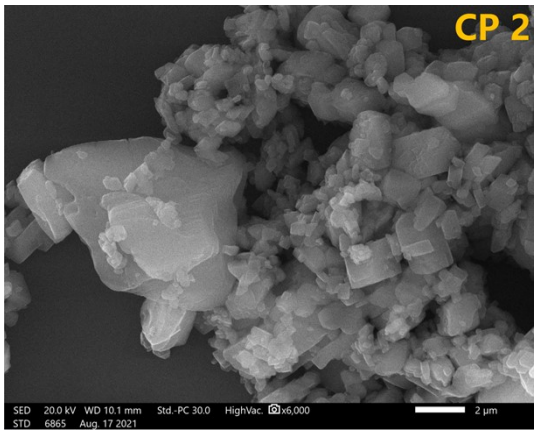

(b)

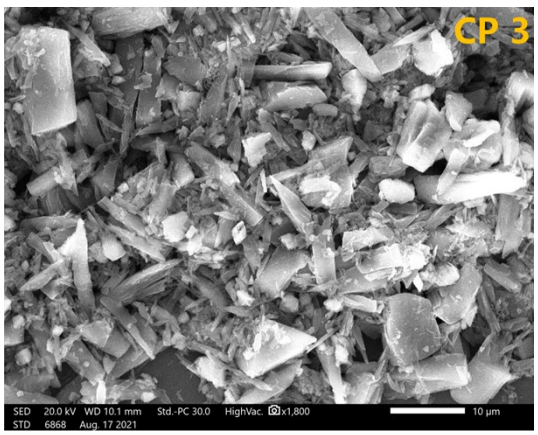

(c)

Fig. S2 Image obtained by SEM of ground samples of CP **1** (a), CP **2** (b) and CP **3**(c) after ball-milled.

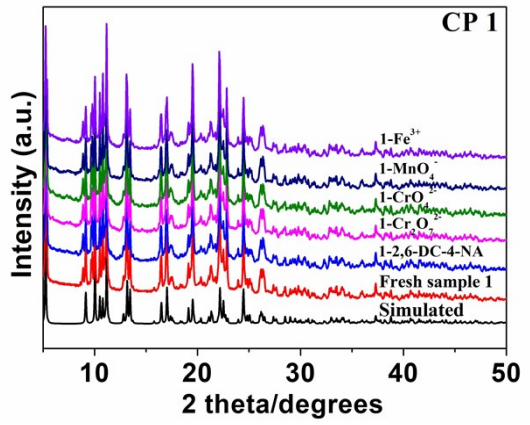

(a)

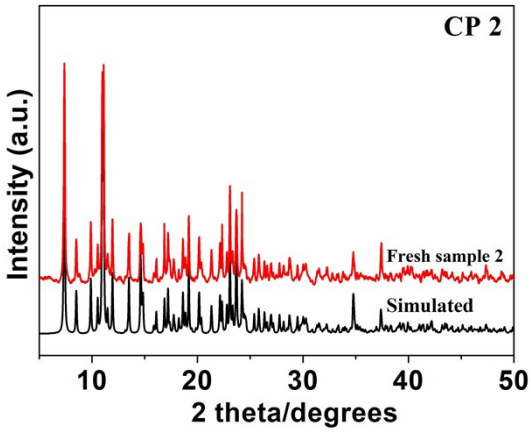

(b)

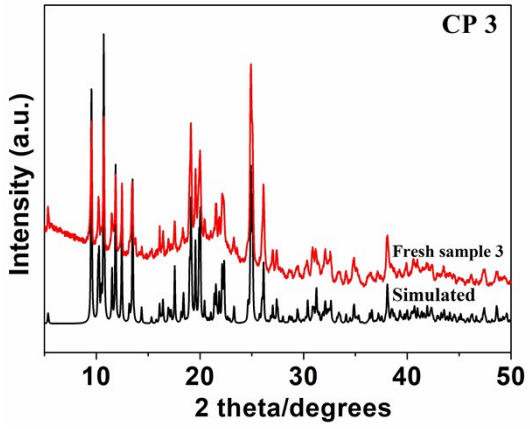

(c)

Fig. S3 The PXRD patterns of CPs **1**–**3**.

As shown in Fig. S3, the peak position of diffraction peak obtained by single crystal fitting is basically consistent with the peak position of bulk material measured by experiment, which shows that the purity of bulk material is good. After soaking in analytes solutions (Fe^{3+}, MnO_4^-, CrO_4^{2-}, $Cr_2O_7^{2-}$ and 2,6-DC-4-NA) for 24 hours, the PXRD patterns of **1** were basically consistent with the original spectra, which show the good stability and recoverability during the fluorescent process.

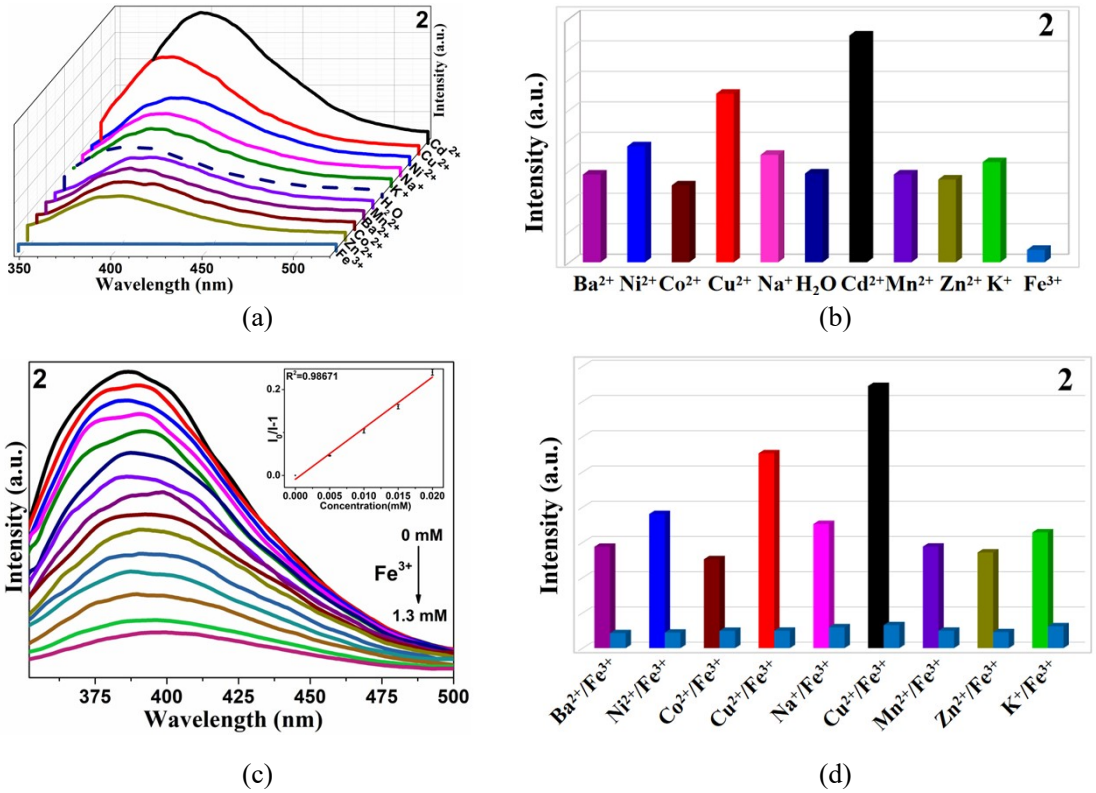

Fig. S4 (a) Fluorescence intensity spectra of CP **2** dispersed in different metal cations (Waterfall plot). (b) Emission intensity of CP **2** in various metal cations (Histogram). (c) Adding Fe^{3+} solutions with different volumes (concentrations of 10^{-3} M), the fluorescence intensity of CP **2** (Inset: At low concentrations, linear relationship between $I_0/I - 1$ and analyte concentration). (d) The selectivity of CP **2** to Fe^{3+} solution is interfered by other metal cations.

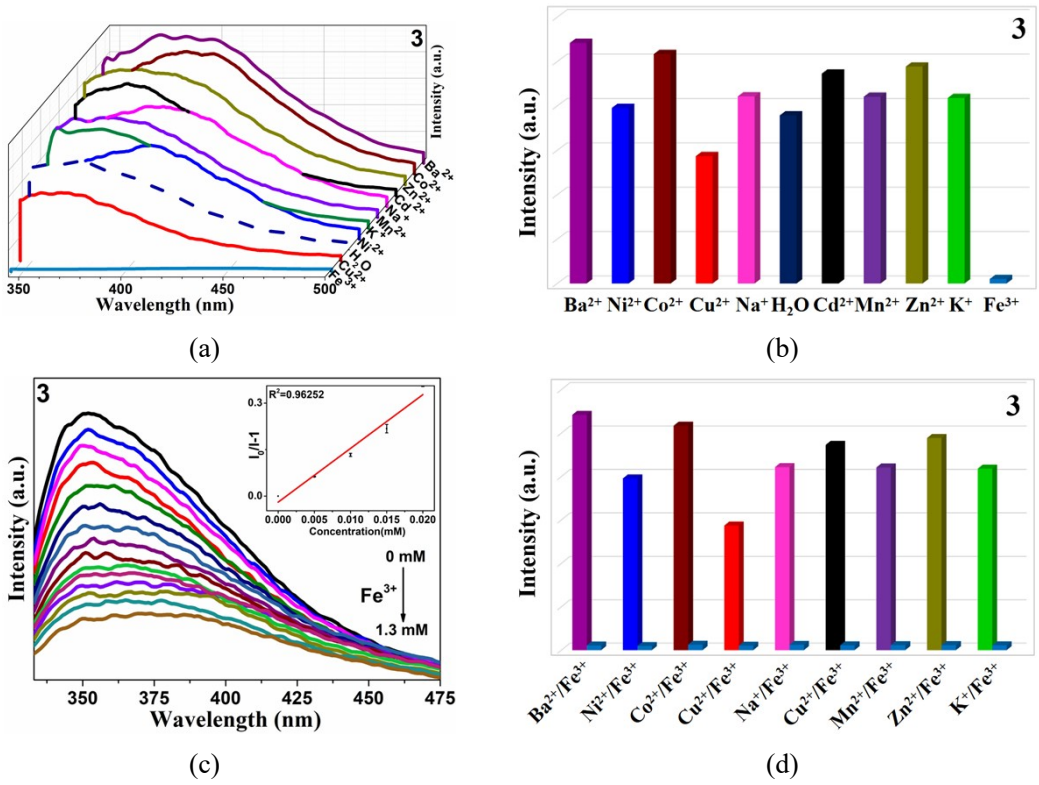

Fig. S5 (a) Fluorescence intensity spectra of CP **3** dispersed in different metal cations (Waterfall plot). (b) Emission intensity of CP **3** in various metal cations (Histogram). (c) Adding Fe^{3+} solutions with different volumes (concentrations of 10^{-3} M), the fluorescence intensity of CP **3** (Inset: At low concentrations, linear relationship between $I_0/I - 1$ and analyte concentration). (d) The selectivity of CP **3** to Fe^{3+} solution is interfered by other metal cations.

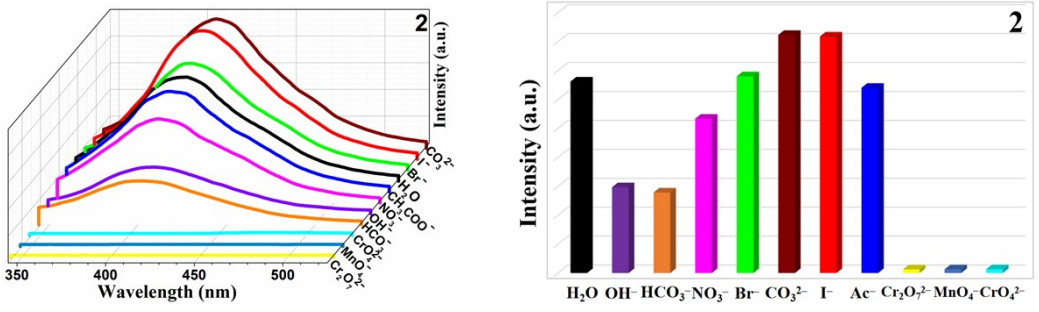

Fig. S6 (a) Fluorescence intensity spectra of CP **2** dispersed in different anions (Waterfall plot). (b) Emission intensity of CP **2** in various anions (Histogram).

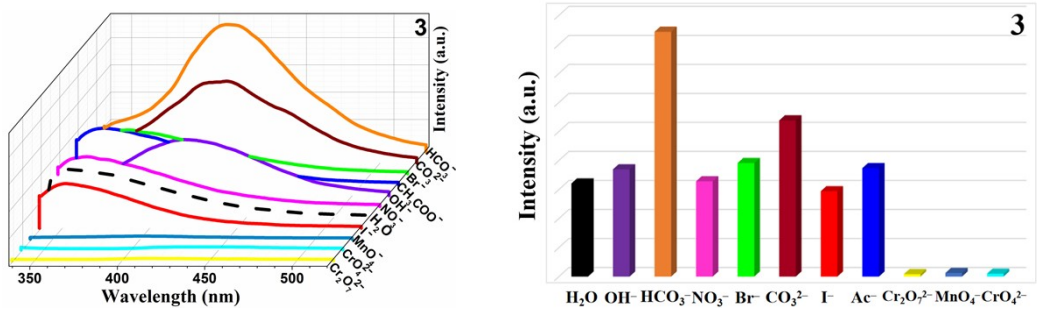

(a) (b)

Fig. S7 (a) Fluorescence intensity spectra of CP **3** dispersed in different anions (Waterfall plot). (b) Emission intensity of CP **3** in various anions (Histogram).

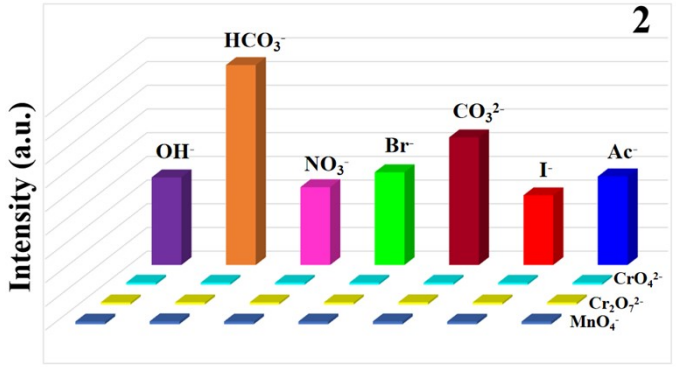

Fig. S8 The anti-interference experiment of CP **2**, in the presence of MnO_4^-, CrO_4^{2-} and $Cr_2O_7^{2-}$ solutions.

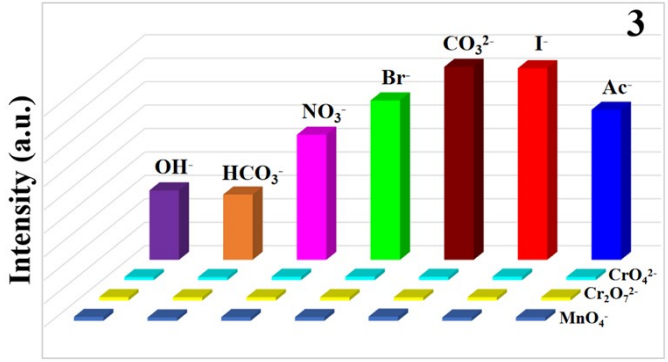

Fig. S9 The anti-interference experiment of CP **3**, in the presence of MnO_4^-, CrO_4^{2-} and $Cr_2O_7^{2-}$ solutions.

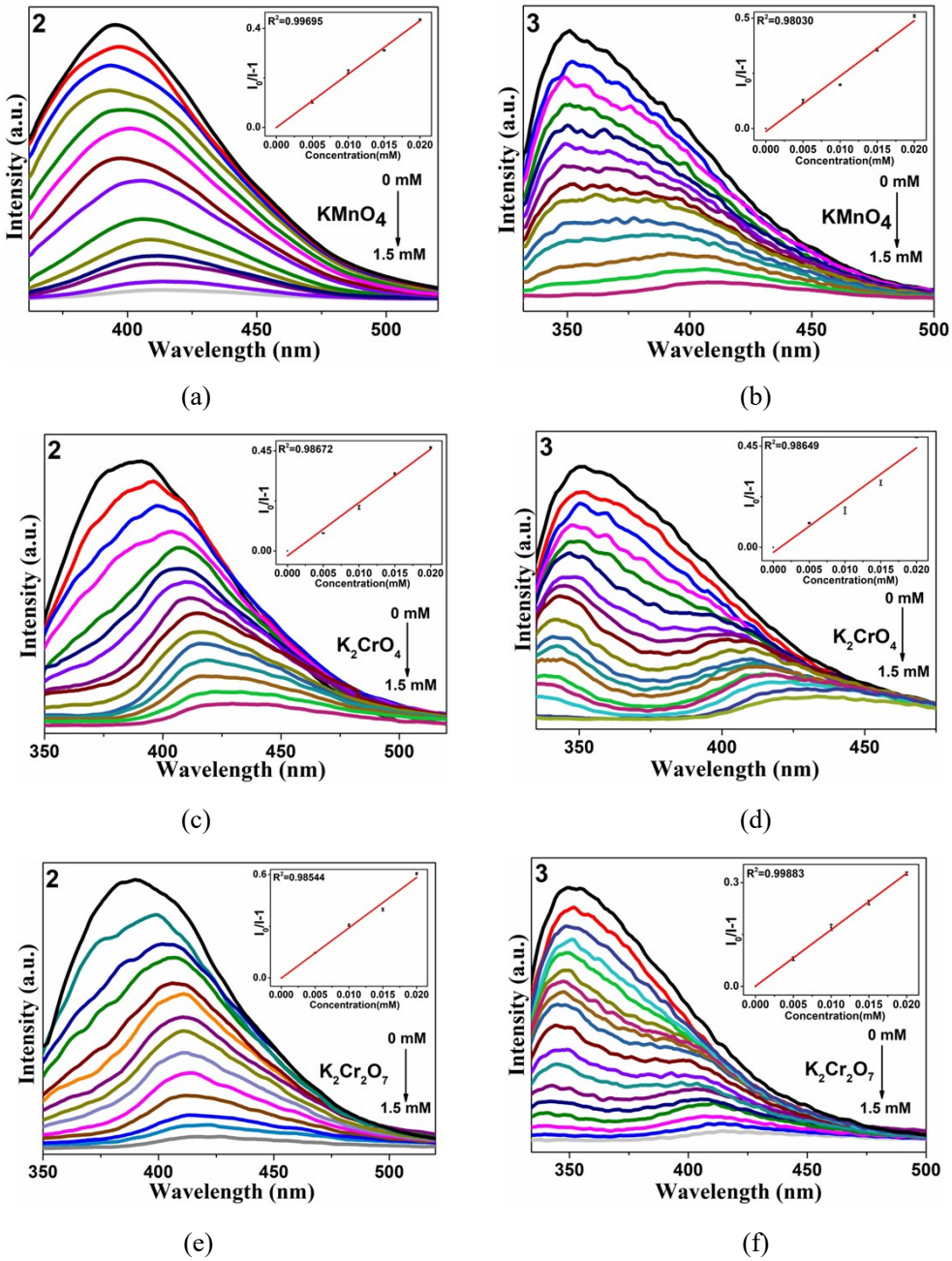

Fig. S10 The fluorescence intensity of CPs **2** and **3**, adding MnO_4^- (a) and (b), CrO_4^{2-} (c) and (d), $Cr_2O_7^{2-}$ (e) and (f) solutions with different volumes and concentrations of 10^{-3} M (Inset: At low concentrations, linear relationship between $I_0/I - 1$ and analyte concentration).

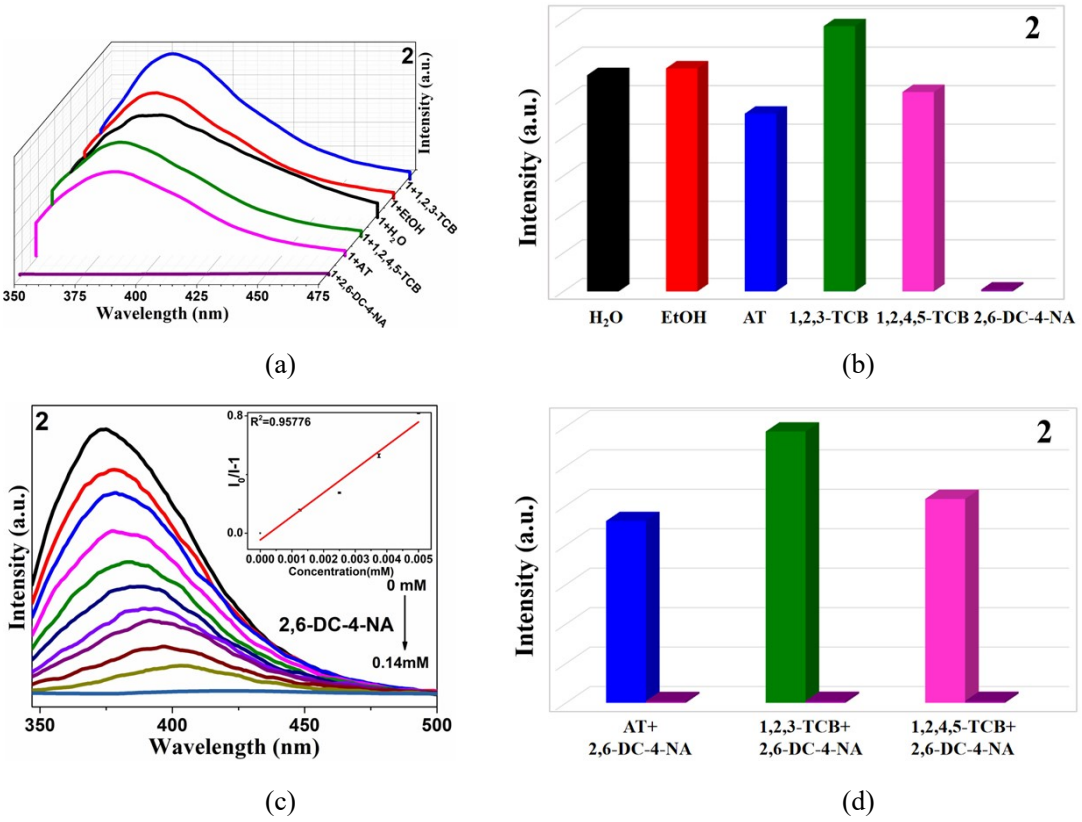

Fig. S11 (a) Fluorescence intensity spectra of CP **2** dispersed in several pesticides (Waterfall plot). (b) Emission intensity of CP **2** in different pesticides (Histogram). (c) Fluorescence spectra of CP **2** to pesticides with different volumes in ethanol solution (Inset: At low concentrations, linear relationship between $I_0/I - 1$ and analyte concentration). (d) The anti-interference experiment.

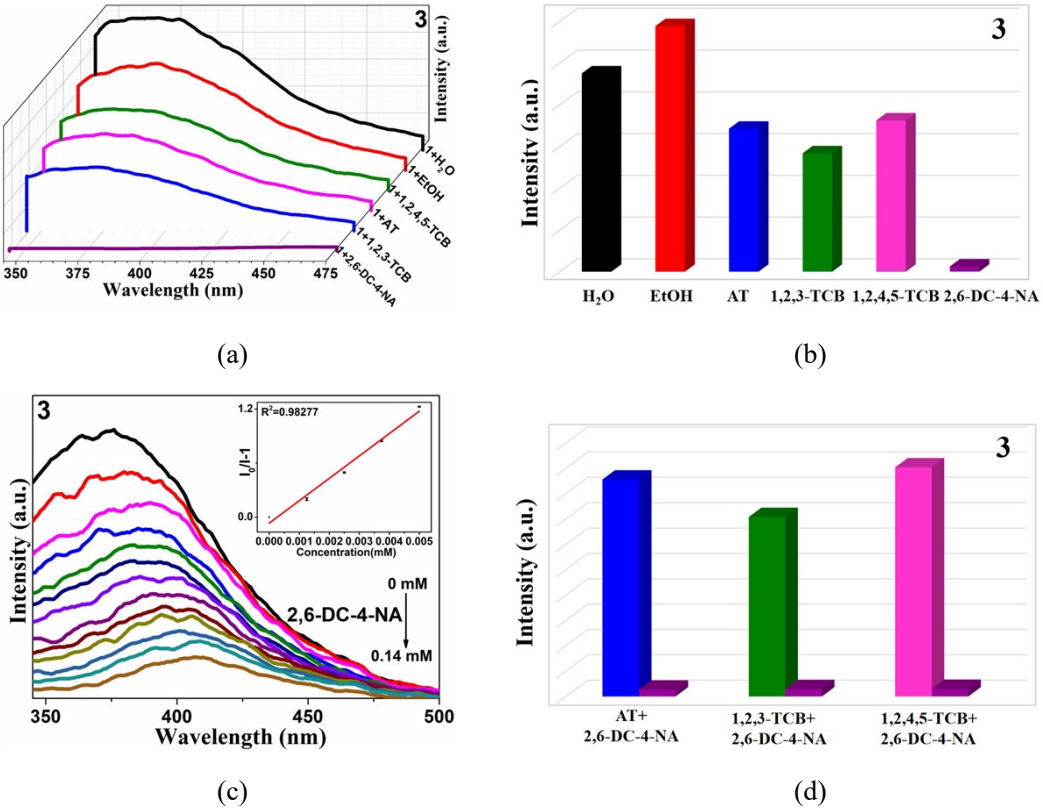

Fig. S12 (a) Fluorescence intensity spectra of CP **3** dispersed in several pesticides (Waterfall plot). (b) Emission intensity of CP **3** in different pesticides (Histogram). (c) Fluorescence spectra of CP **3** to pesticides with different volumes in ethanol solution (Inset: At low concentrations, linear relationship between $I_0/I - 1$ and analyte concentration). (d) The anti-interference experiment.

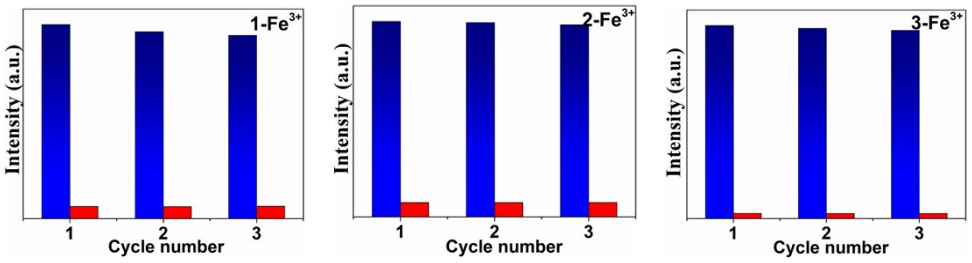

(a)

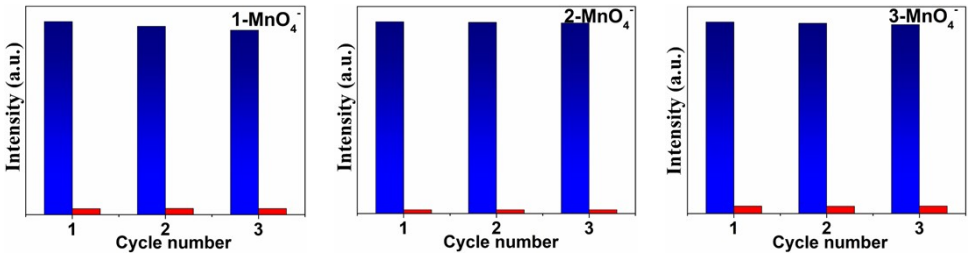

(b)

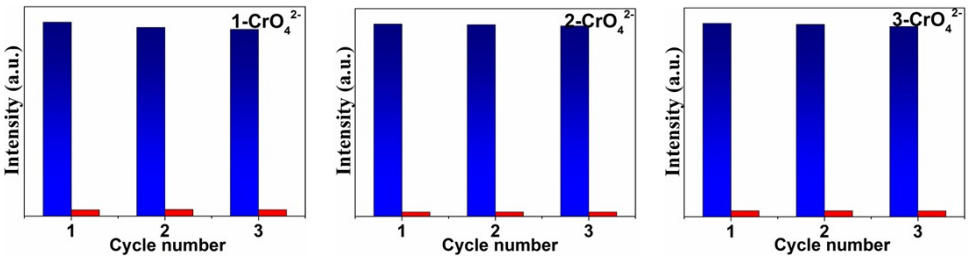

(c)

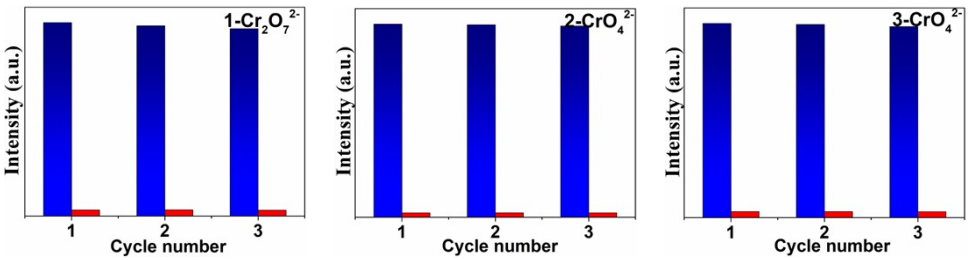

(d)

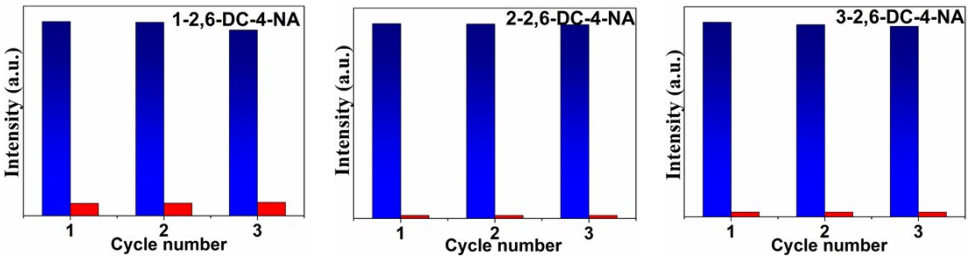

(e)

Fig. S13 (a)–(e) Cyclic experiments of CPs **1**–**3**, blue is the original intensity, red is the fluorescence intensity after adding five analytes.

Table S4. Comparison of different coordination polymers for detection of Fe^{3+}.

Coordination polymers	Quenching constant Ksv (M^{-1})	The detection limit (μM)	Reference
$[Pb(L)_2]_n$	1.01×10^4		S9
$\{[Ca_3L_2(H_2O)_6]\cdot 2H_2O\}_n$	3737.8	1040	66
$\{[Cd_2(DDPP)(DMF)(H_2O)]\cdot DMF\}_n$	3.98×10^4	477	67
$[Cu_3L]_n$	9.47×10^3	998	68
$\{[Zn_2(\mu_4\text{-}L)(\mu\text{-dpetan})_2]\cdot 2H_2O\}_n$	2.404×10^3	210	S10
$[Cd(L)(ADI)]\cdot H_2O$	1.202×10^4	630	this work
$[Cd(L)(PIM)]\cdot H_2O$	1.189×10^4	710	this work
[Cd(L)(SUB)]	1.734×10^4	730	this work

Table S5. Comparison of different coordination polymers for detection of anions.

Coordination polymers	Analytes	Quenching constant Ksv (M^{-1})	The detection limit (μM)	Reference
$[Zn(L)_2]\cdot 2DMF$ (USTC-5)	MnO_4^-	1.92×10^4	23.4	69
$\{[Co(TCPA)(L)]\cdot H_2O\}_n$	$Cr_2O_7^{2-}/CrO_4^{2-}$	$1.43/1.24 \times 10^4$	0.06/0.21	70
$[EuL(CH_3COO)Cl]_n$	$Cr_2O_7^{2-}/CrO_4^{2-}$	$1.15/2.52 \times 10^4$	86.3/85.4	74
$[Cd(L)(HIPA)(H_2O)]\cdot H_2O$	$MnO_4^-/Cr_2O_7^{2-}/CrO_4^{2-}$	$1.17/1.08/1.03 \times 10^4$	256/278/291	S11
$[Zn(L)_2]_n$	$Cr_2O_7^{2-}/CrO_4^{2}$	$4.454/1.161 \times 10^4$	0.67/2.56	S12
$[Cd(L)(ADI)]\cdot H_2O$	$MnO_4^-/Cr_2O_7^{2-}/CrO_4^{2-}$	$1.794/3.055/1.987 \times 10^4$	420/250/380	This work
$[Cd(L)(PIM)]\cdot H_2O$	$MnO_4^-/Cr_2O_7^{2-}/CrO_4^{2-}$	$2.158/2.922/2.399 \times 10^4$	390/290/350	This work
[Cd(L)(SUB)]	$MnO_4^-/Cr_2O_7^{2-}/CrO_4^{2-}$	$2.506/1.629/2.323 \times 10^4$	510/780/550	This work

Table S6. Comparison of different coordination polymers for detection of 2,6-DC-4-NA.

Coordination polymers	Quenching constant Ksv (M^{-1})	The detection limit (μM)	Reference
$[Zn(L)(1,4\text{-BDC})]\cdot H_2O$	2.78×10^4	119	23
$[Zn(L)(1,3\text{-BDC})]\cdot H_2O$	4.88×10^4	68	23
$[Zn_2(L)_2(IP)]_2$	3.9×10^4	67	55
Zn-NDC-MI	2.9×10^4	0.06	73
$[Cd(L)(ADI)]\cdot H_2O$	1.334×10^5	57	This work
$[Cd(L)(PIM)]\cdot H_2O$	1.609×10^5	52	This work
[Cd(L)(SUB)]	2.483×10^5	51	This work

Table S7. The repeated test and relative standard deviation of detection limit of CP **1**.

Test	Fe^{3+}	MnO_4^-	CrO_4^{2-}	$Cr_2O_7^{2-}$	2,6-DC-4-NA
Test 1	630	420	380	250	57
Test 2	618	430	389	248	57
Test 3	625	429	385	251	56
Mean (μM)	624	426	384	250	57
RSD (%)	0.97	1.29	1.17	0.61	1.02

Table S8. The repeated test and relative standard deviation of detection limit of CP **2**.

Test	Fe^{3+}	MnO_4^-	CrO_4^{2-}	$Cr_2O_7^{2-}$	2,6-DC-4-NA
Test 1	710	390	350	290	52
Test 2	704	392	351	285	52
Test 3	715	399	355	290	53
Mean (μM)	710	394	352	288	52
RSD (%)	0.78	1.20	0.75	1.00	1.10

Table S9. The repeated test and relative standard deviation of detection limit of CP **3**.

Test	Fe^{3+}	MnO_4^-	CrO_4^{2-}	$Cr_2O_7^{2-}$	2,6-DC-4-NA
Test 1	730	510	550	780	51
Test 2	727	510	545	772	51
Test 3	734	524	550	791	52
Mean (μM)	730	515	548	781	51
RSD (%)	0.48	1.57	0.53	1.22	1.13

References

[S1] M. Sarkar, K. Biradha, Cryst. Growth Des., 2006, 6, 202–208.

[S2] C. D. Si, D. C. Hu, Y. Fan, Y. Wu, X. Q. Yao, Y. X. Yang, J. C. Liu, Cryst. Growth Des., 2015, 15, 5, 2419–2432.

[S3] Y. J. Mu, Y. G. Ran, B. B. Zhang, J. L. Du, C. Y. Jiang, J. Du, Cryst. Growth Des., 2020, 20, 9, 6030–6043.

[S4] B. Dutta, A. Hazra, A. Dey, C. Sinha, P. P. Ray, P. Banerjee, M. H. Mir, Cryst. Growth Des., 2020, 20, 2, 765–776.

[S5] S. S. Chen, Z. Y. Zhang, R. B. Liao, Y. Zhao, C. Wang, R. Qiao, Z. D. Liu, Inorg. Chem., 2021, 60, 7, 4945–4956.

[S6] L. N. Zhu, Z. P. Deng, S. W. Ng, L. H. Huo, S. Gao, Dalton Trans., 2019, 48, 7589–7601.

[S7] B. Dolenský, R. Konvalinka, M. Jakubek, V. Král, J. Mol. Struct., 2013, 1035, 124–128.

[S8] L. Yang, F. Wang, D. Y. Auphedeous, C. L. Feng, Nanoscale, 2019, 11, 14210–14215.

[S9] L. Yi, F. Guo, Aust.J.Chem., 2020, 73, 21–29.

[S10] T. A. Arici, O. Z. Yesilel, M. Arici, J. Taiwan, Inst. Chem. E., 2020, 114, 300–310.

[S11] G. C. Liu, Y. Li, J. Chi, N. Xu, X. L. Wang, H. Y. Lin, B. K. Chen, J. R. Li, Dalton Trans., 2020, 49, 737–749.

[S12] T. Y. Xu, H. J. Nie, J. M. Li, Z. F. Shi, J. Solid. State. Chem., 2020, 287, 121342.